福昕PDF编辑器

• 永久　• 轻巧　• 自由

升级会员　　批量购买

永久使用

无限制使用次数

极速轻巧

超低资源占用，告别卡顿慢

自由编辑

享受Word一样的编辑自由

扫一扫，关注公众号

Tiny and Dim Infrared Target Detection Based on Weighted Local Contrast

Jie Liu, Ziqing He, Zuolong Chen, and Lei Shao

***Abstract*— Robust detection of infrared (IR) tiny and dim targets in a single frame remains a hot and difficult problem in military fields. In this letter, we introduce a method for IR tiny and dim target detection based on a new weighted local contrast measure. Our method simultaneously exploits the local contrast of target, the consistency of image background, and the imaging characteristics of the background edges. The proposed method is simple to implement and computationally efficient. We compared our algorithm with six state-of-the-art methods on four real-world videos with different targets and backgrounds. Our method outperforms all the compared algorithms on the ground-truth evaluation with both higher detection rate and lower false alarm rate.**

***Index Terms*— Infrared (IR) image, tiny and dim target detection, weighted local contrast measure.**

I. Introduction

INFRARED imaging and detection techniques are widely used in military surveillance, targeting, detection, and navigation [1] because of their unique superiorities. Small and dim IR target detection plays a crucial role in these applications. However, for the small and dim IR targets, such as aircraft, missiles, ships, and shells, there still exist three challenges to detect them in real time. First, such targets usually lack shape and texture information due to the far imaging distance. Second, such targets often conceal in strong background clutters. Third, the imaging backgrounds usually change fast since such targets always have very high velocities [2].

Small and dim IR target detection methods can be roughly classified into sequential detection methods and single-frame detection approaches [2]. Sequential detection methods utilize spatial-temporal information [3] and perform well for static background given some prior knowledge on targets [2]. However, the performance degrades rapidly when the imaging background changes quickly [4].

In contrast, single-frame detection approaches detect targets in a single frame directly. For example, methods [5]–[7] put emphasis on estimating the image background and then use the difference between the original image and the estimated background to realize target detection. Deshpande *et al.* [5] make use of the max-mean/max-median filters to estimate the image background. Unlike the traditional morphology-based algorithm [6], Bai and Zhou [7] use the morphological opening operation with two newly defined structuring elements to estimate the image background.

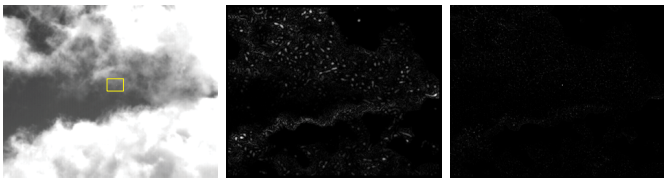

(a) (b) (c)

Fig. 1. We use a novel weighted local contrast measure to filter the original image. Compared with the result of IDoGb [12], our result has less background clutters, and the target is correctly enhanced. (a) Source. (b) Result of IDoGb [12]. (c) Our result.

Different from the background estimation methods, low-rank methods [2], [4], [8], which exploit the target sparse prior and background low-rank prior, formulate the target detection as an optimization problem of recovering low-rank and sparse matrices. Gao *et al.* [2] and He *et al.* [8] assume that all the background patches come from a single low-rank subspace and a mixture of several low-rank subspaces, respectively. Dai and Wu [4] combine the local structure and background low-rank priors together to improve the detection performance.

Inspired by the contrast mechanism of human visual system (HVS), some target detection methods focus on constructing a local contrast map, which indicates the dissimilarity between the local pixel/pixels and its/their neighborhoods, and adopt an adaptive threshold to segment the target. The contrast mechanism can be simulated using Laplacian of Gaussian [1], [9], difference of Gaussians [10], [11], and improved difference of Gabor [12] filters. In addition, some algorithms [13]–[16] directly introduce specific local contrast measures to construct the local contrast map.

In summary, all the above-mentioned algorithms are rooted in the local contrast of target or/and the consistency of the image background. When the image background is simple or there is a great local contrast of target, these algorithms can achieve satisfying performance. However, when they come to images with heavily cluttered background and tiny dim targets, their performances decline significantly. It is also found that the false alarms of such algorithms come mainly from the edges of the heavy clutters [Fig. 1(b), see the Supplemental Material for graphs]. Therefore, in order to dramatically reduce false alarms, this letter not only takes advantage of the local contrast of target, the consistency of background but also takes into account the imaging characteristics of the clutter edges, which greatly reduces false alarms [see Fig. 1(c)]. A new local

Manuscript received February 1, 2018; revised June 26, 2018; accepted July 9, 2018. *(Corresponding author: Jie Liu.)*

J. Liu, Z. He, and Z. Chen are with the Department of Test, Baicheng Ordnance Test Center of China, Baicheng 137001, China (e-mail: liu1977jie@sina.com).

L. Shao is with the Ministry of Security, Beijing Space Information Relay Transmission Technology Research Center, Beijing 100094, China.

Color versions of one or more of the figures in this letter are available online at http://ieeexplore.ieee.org.

Digital Object Identifier 10.1109/LGRS.2018.2856762

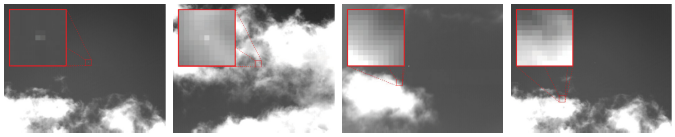

(a) (b) (c) (d)

Fig. 2. (a) and (b) Imaging characters of the tiny dim IR targets. (c) and (d) Edges of the strong clutters. The local regions of the targets and the edges are magnified in the large red box.

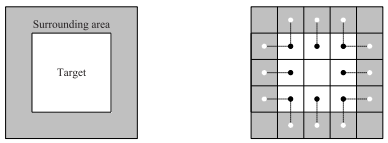

(a) (b)

Fig. 3. (a) Target region and its surrounding area. (b) Corresponding pixel pairs (each cell represents a pixel) in them.

contrast measure (NLCM) is first proposed according to the imaging character of IR tiny target, by which the strong background clutters are well suppressed. Then, based on the imaging characteristics of the clutter edges, the probability of a pixel belonging to a target is estimated and used as the weight factor of NLCM; thus, a weighted local contrast map is generated, and the edge of the strong clutter is further suppressed. Finally, a robust target detection method can be achieved by a simple threshold segmentation on the weighted local contrast map.

II. Proposed Method

A. New Local Contrast Measure

1) Imaging Characteristic of the Tiny and Dim Target: In general, tiny and dim IR target always has very low contrast. However, the gray level of a tiny and dim IR target would stand out relative to its neighborhood. As shown in Fig. 2(a), there is a large area of high radiant clouds at the bottom of the image, and the target is low in brightness. But in the local region, the gray value of the target is higher than that of its surrounding area. Similarly, in Fig. 2(b), there are lots of highly radiated clouds in the whole image, and the target is almost submerged in the cloud clutters. But the gray value of the target is still higher than that of its local neighborhood.

2) New Local Contrast Measure: According to Section II-A1, the IR target is generally prominent in its neighborhood which means that there is a local difference between the target and its surrounding region. References [13]–[16] have achieved fairly good performance by using the center-surround (C-S) difference. However, the computational complexities of the C-S difference measures they used are high. Here, we present an NLCM that is simple and easy to calculate.

As shown in Fig. 3(a), the white area is assumed as a target region which contains M pixels. Correspondingly, the gray area is the surrounding area of the target which contains N pixels. For the pixel intensity $I(x, y)$ in the target, the average gray values of the target and its surrounding area are denoted by $m_t(x, y) = (1/M)\sum_{j=1}^{M} I_j$ and $m_s(x, y) = (1/N)\sum_{j=1}^{N} I_j$, respectively. Then, the NLCM of the pixel

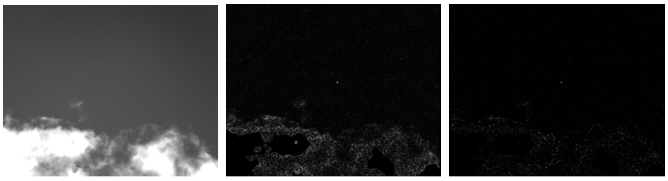

(a) (b) (c)

Fig. 4. Original image and its local contrast map and weighted local contrast map obtained by using (1) and (3), respectively. (a) Original. (b) Result of NLCM. (c) Result of WLCM.

intensity $I(x, y)$ is defined as

$$D(x, y) = |m_t(x, y) - m_s(x, y)|. \tag{1}$$

In real-world applications, the width of the surrounding area is only one pixel, *e.g.*, when $M = 1$, $N = 8$. By processing an input image with (1) by means of convolution, we get the local contrast map [see Fig. 4(b)] of the original image efficiently.

B. Foreground Weighting

1) Imaging Characteristic of the Clutter Edges: Taking the IR sky background as an example, cloud is generally the main background clutter. As shown in Fig. 2(c) and (d), the gray values of the interior pixels of the clouds are saturated owing to the limited bit depth of the image. However, the edges of the strong cloud clutters would have prevailing orientations, which are quite distinct from the target [see Fig. 2(a) and (b)]. On the other hand, as can be seen from Fig. 4(b), the NLCM defined by (1) is greatly influenced by the cloud clutter edges, which produce lots of noises. Therefore, further suppression of the clutter edges would lead to further reduction of the false alarm rate.

2) Foreground Weighting: From Section II-B1, we can draw the following conclusion: if a pixel or a region has higher gray level pixels in its neighborhood, then the pixel or the region is more likely to be on the clutter edge. Therefore, it is potential to estimate the probability of a pixel belonging to foreground (target) by comparing the gray values of the central region with its surrounding pixels.

As shown in Fig. 3(b), the white area is the target region whose center is pixel $I(x, y)$, and the gray area is its surrounding area. We first compare the gray values of the outermost pixels in the white region with their four-neighborhood gray pixels [the black-white pixel pairs in Fig. 3(b)], and suppose that there is a total of k pairs in all the pixel pairs, which satisfy that the gray pixel's value is greater than or equal to that of the white pixel's value. Then, the probability of the pixel $I(x, y)$ belonging to the target is defined as

$$W(x, y) = \frac{1}{1 + k^2}. \tag{2}$$

Combining (1) and (2), the weighted new local contrast measure (WLCM) of the pixel intensity $I(x, y)$ is calculated by

$$I_{\text{out}}(x, y) = D(x, y) \times W(x, y). \tag{3}$$

According to (3), a weighted local contrast map can be obtained by computing the WLCM of all the pixels in the original image, which is shown in Fig. 4(c).

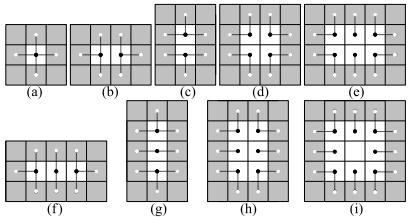

Fig. 5. Multiscale neighborhood structure diagram. Each cell represents a pixel, and the black-white point pairs are the pixel pairs that need to be considered in computing k in (2). (a) 3×3. (b) 3×4. (c) 4×3. (d) 4×4. (e) 4×5. (f) 3×5. (g) 5×3. (h) 5×4. (i) 5×5.

C. Multiscale WLCM

We experimentally find that if the target imaging is clear, even if the target size has a great change in a certain range, the single-scale WLCM can achieve good detection results. However, when the target imaging is blurry, the gray level of the target is not a Gaussian distribution, and the target in the image may be a patch with the same or similar gray values. At this point, if the white region in Fig. 3 is too small or too large, it is difficult for single-scale WLCM to detect the target correctly, because (3) cannot get its maximum value. Therefore, in practical applications, a multiscale neighborhood structure can be adopted according to the target size. Fig. 5 is a basic multiscale neighborhood structure representation.

Assuming $I_{\text{out}1}(x, y)$, $I_{\text{out}2}(x, y), \ldots, I_{\text{out}N}(x, y)$ are the WLCM values corresponding to the N neighborhood structures of the pixel $I(x, y)$, the output result of the multiscale WLCM (MWLCM) of the pixel $I(x, y)$ is defined as

$$I_{\text{out}}(x, y) = \max(I_{\text{out}1}(x, y), I_{\text{out}2}(x, y), \ldots, I_{\text{out}N}(x, y)). \tag{4}$$

D. Target Detection

Overall, the maps calculated by WLCM [see (3)] and MWLCM [see (4)] can greatly suppress the strong background clutters and enhance the target simultaneously. Higher gray value of a pixel in the map [see Fig. 4(c)] indicates larger probability of a target. Therefore, the target detection can be realized by using a simple segmentation method on the map, where the adaptive threshold T is defined as

$$T = \alpha \overline{I} + (1 - \alpha) I_{\max} \tag{5}$$

where $\overline{I}$ and $I_{\max}$ are the average and maximum values of the WLCM (MWLCM) map, respectively, and α is a constant. In this letter, α is 0 for single-target detection and 0.92 for multitarget detection.

E. Algorithm Acceleration

Calculating the weight factor $W(x, y)$ [see (2)] for all the pixels is time-consuming and unnecessary. If the NLCM of a pixel is relatively small, in Section II-A2, it has been analyzed that the pixel is less likely to be a target, so there is no need to calculate its $W(x, y)$. Therefore, (3) can be rewritten as

$$I_{\text{out}}^{\text{acc}}(x, y) = \begin{cases} D(x, y) \times W(x, y) & \text{for } D(x, y) \geq T_D \\ D(x, y) & \text{for } D(x, y) < T_D \end{cases} \tag{6}$$

where T_D is defined as

$$T_D = \beta \overline{D} + (1 - \beta) D_{\max} \tag{7}$$

where $\overline{D}$ and $D_{\max}$ are the average and maximum values of the NLCM map, and β is a constant.

It can be seen from (6) that the computational complexity of the algorithm can be greatly reduced since only the pixels with high gray value are weighted.

III. Experiment and Comparison

In order to verify the effectiveness of our method, we selected four typical IR video sequences from real-world applications. For the selected sequences, each frame is first annotated by one person. Then, it is checked and modified by another person to ensure the correctness of the annotation. Finally, the annotation results are used as benchmark (ground truth). The characteristics of each sequence are shown in Table I. A typical frame of each sequence is shown in Fig. 6.

We compare our algorithm with six most relevant state-of-the-art algorithms, which are improved difference of Gabor (IDoGb) [12], weighted local difference measure (WLDM) [13], multiscale patch-based contrast measure (MPCM) [16], modified new white top-hat transformation (MNWTH) [7], maxMedian [5], and maxMean [5], respectively. We select these algorithms for comparison with consideration of the following reasons: citation in the literature (the classic approach of MNWTH, maxMedian, and maxMean are widely cited), recency (IDoGb and WLDM are recent), and variety (MNWTH, maxMedian, and maxMean are background estimation motivated. IDoGb, WLDM, and MPCM are the HVS-based methods). At the same time, our algorithm is represented by four models: WLCM, MWLCM, accelerated weighted local contrast measure (AWLCM), and accelerated multiscale weighted local contrast measure (AMWLCM). Among them, WLCM and AWLCM denote single-scale nonacceleration and acceleration models using Fig. 5(a) neighborhood structure and MWLCM and AMWLCM denote multiscale nonacceleration and acceleration models using Fig. 5(a)–(d) four neighborhood structures, respectively. Since all the authors of the above-mentioned algorithms do not disclose their relevant codes, all the algorithms are programmed by ourself in the MATLAB environment.

A. Evaluation Metrics

1) Detection Rate, False Alarm Rate, and ROC Curve: In the small and dim IR target detection, after getting the transformed (filtered) map, the potential target can be segmented by a certain threshold. Then, the same as [2] and [13], the detection rate P_d and the false alarm rate F_a are calculated according to ground truths

$$P_d = \frac{\#\text{ number of true detections}}{\#\text{ number of actual targets}} \tag{8}$$

$$F_a = \frac{\#\text{ number of false detections}}{\#\text{ number of images}}. \tag{9}$$

We follow the evaluation protocol in [2], where the detection result is considered correct when the result meets the following two criteria simultaneously: 1) the result has overlapping pixels with the ground truth and 2) the distance between the result and the center of the ground truth is within 4 pixels. By changing the segmentation threshold, we can get different

TABLE I

CHARACTERISTICS OF FOUR TYPICAL IR VIDEO SEQUENCES

	#Frame	Resolution(pixel)	Target size (pixel)	#Target	Background details	Target details
Seq. 1	300	320×256	1∼4	1	•Relatively homogeneous.	•Keeping motion.
Seq. 4	40	320×256	1∼15	30∼50	•Heavy noise.	•Low contrast.
Seq. 2	300	320×256	1∼4	1	•Heavily cloudy clutter background.	•Low signal-to-clutter ratio.
Seq. 3	545	320×256	4∼12	1	•Changing backgrounds.	

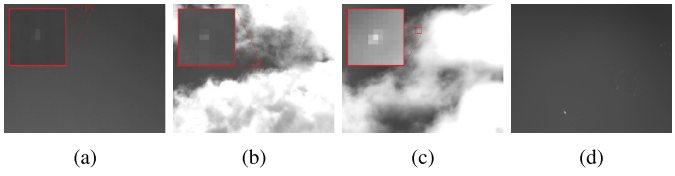

(a) (b) (c) (d)

Fig. 6. Representative frames of the four real-world video sequences. (a) Seq. 1. (b) Seq. 2. (c) Seq. 3. (d) Seq. 4.

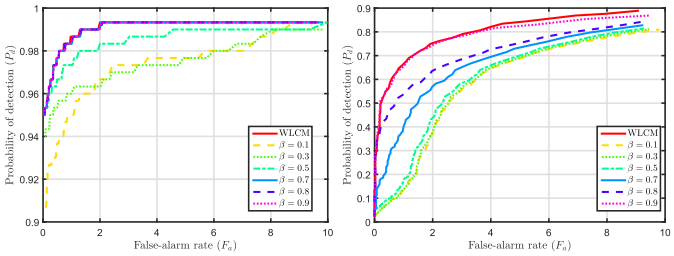

(a) (b)

Fig. 7. Evaluation of WLCM and its acceleration model (AWLCM) with different β values in (7) on (a) Seq. 2 and (b) Seq. 4.

TABLE II

RUNNING TIME OF WLCM AND ITS ACCELERATION MODEL

Method	WLCM	AWLCM with different β					
		$\beta = 0.1$	$\beta = 0.3$	$\beta = 0.5$	$\beta = 0.7$	$\beta = 0.8$	$\beta = 0.9$
Time(s)	0.8838	0.0011	0.0011	0.0014	0.0030	0.0071	0.0257

P_d and F_a values for each frame. Then, the receiver operating characteristic (ROC) curves are plotted based on the average of P_d and F_a on all the video frames.

B. Effects of Parameter β

We evaluate the performance of WLCM and AWLCM with different β values in (7) on Seqs. 1∼4. As shown in Fig. 7 and Table II, evaluation results on different sequences have similar characteristics: 1) larger β brings higher P_d with longer computational time and 2) when β is greater than 0.7 for single and 0.9 for multitarget sequences, P_d of the acceleration model is very close to P_d of the nonacceleration model. Therefore, in order to take into account both P_d and computational complexity, β is set 0.8 for single and 0.9 for multitarget sequence, respectively, in the following experiments.

C. Comparison With the State of the Art

1) ROC: First, all the algorithms are tested on all the sequences. According to Section III-A, the ROC curves are computed and shown in Fig. 8.

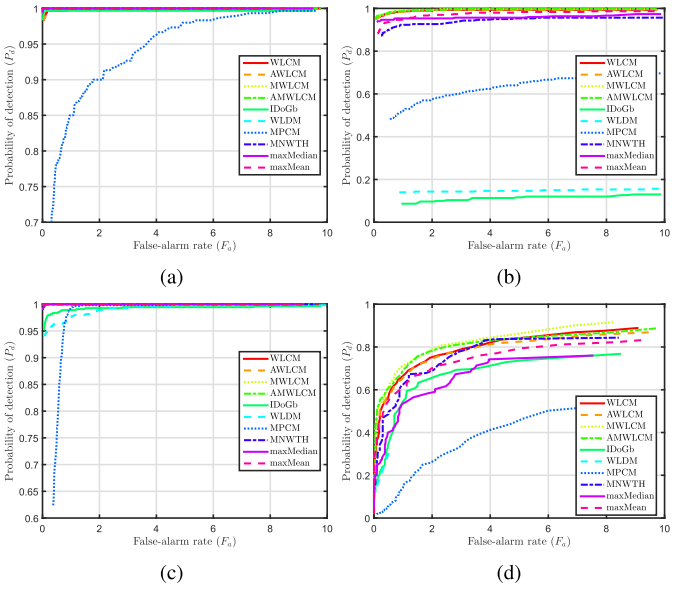

(a) (b) (c) (d)

Fig. 8. ROC curves of 10 methods on the four video sequences. (a) Seq. 1. (b) Seq. 2. (c) Seq. 3. (d) Seq. 4.

As can be seen from Fig. 8(a), owing to the relatively homogeneous background of Seq. 1, all the algorithms except MPCM [16] get high P_d without any false alarms or low F_a. In Seq. 2 [see Fig. 8(b)], the results of our four models are obviously superior to all the other algorithms. The performance of IDoGb [12], WLDM [13], and MPCM [16] are poor due to the small target size, low gray intensity, and strong background clutter. In Seq. 3 [see Fig. 8(c)], although the background is complex, but the intensity of the target is high and the size of the target is large, except IDoGb [12], WLDM [13], and MPCM [16], all the other algorithms have achieved good results. In particular, our four models have achieved the best result: F_a is 0 and P_d is 1. In Seq. 4, there are about 30 $\sim$ 50 targets in each frame with large size difference. Furthermore, the targets in some frames have motion blur. All of them contribute to a significant decline in P_d for all the algorithms [see Fig. 8(d)], but the result of MWLCM is obviously superior to other algorithms, which shows the effectiveness of our proposed multiscale method.

In Fig. 8(b), the results of our four models are almost overlapped, indicating that the accelerated method proposed in this letter does not significantly reduce P_d. From Fig. 8(b) and (c), we can see that although the target sizes of Seqs. 2 and 3 are different, the performance of the single-scale algorithms (WLCM and AWLCM) are not significantly lower than that of the multiscale algorithms (MWLCM and AMWLCM). This is mainly because the imaging of the targets in Seq. 3 is

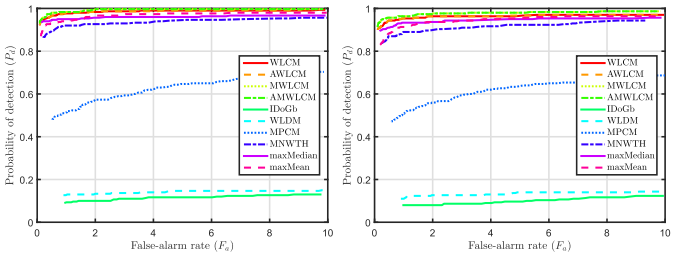

(a) (b)

Fig. 9. ROC curves of different methods on Seq. 2 whose each frame is added Gaussian white noise of different variances, respectively. (a) $\sigma^2_{\text{noise}} = 0.00001$. (b) $\sigma^2_{\text{noise}} = 0.00005$.

TABLE III
COMPARISON OF RUNNING TIME

Method	IDoGb	WLDM	MPCM	MNWTH	maxMedian	maxMean
Time(s)	0.0163	4.4869	0.0215	0.0097	4.5374	4.7010
Method	WLCM	AWLCM	MWLCM	AMWLCM		
Time(s)	0.8838	0.0071	3.5485	0.0504		

relatively clear, and the gray value of the pixels inside the target is higher than that of its outside pixels [see Fig. 6(c)]. Therefore, for such clear imaging targets, even if their size changes obviously, our single-scale models can achieve high P_d, which further illustrates the robustness of our algorithm.

2) Robustness: In order to test the robustness of our algorithm, we add Gaussian white noise of variance 0.00001 and 0.00005 to each frame of Seq. 2 as in [14], respectively. The experimental results are shown in Fig. 9. By comparing Fig. 9 with Fig. 8(b), it is found that the P_d degradations of our models are not obvious when the added noise variance is 0.00001. When the added noise variance is 0.00005, our models are still better than the other algorithms, and the gap between the other algorithms and ours is obviously increased. All these fully demonstrate the robustness of our algorithm to noise.

3) Performance: On all the above-mentioned video sequences with different characteristics, we compared the average running time of all the algorithms on the same computer (Intel Pentium G3260 3.3-GHz CPU and 4-GB RAM). The result is shown in Table III. As can be seen from Table III, the time consumed by the proposed acceleration models is considerably shorter than that of the nonaccelerated models. The time consumed by the single-scale and multiscale acceleration models only accounts for 0.8% and 1.4% of that of the nonacceleration models, respectively. In addition, the time consumed by our single-scale acceleration model AWLCM is obviously lower than all the other algorithms.

All of these experiments show that the proposed algorithm has good robustness and high detection performance. Especially for videos with strong background clutter, tiny and dim targets, and multitargets, the performance of the proposed algorithm is obviously superior to other algorithms.

IV. CONCLUSION

A fast tiny and dim IR target detection algorithm based on the weighted local contrast measure is proposed in this letter. First, an NLCM is introduced according to the imaging characteristics of the IR tiny target. Then, to further suppress the background clutter, a weight factor is defined based on the gradual changing property of the strong clutter edges. Finally, after the weighted local contrast map is obtained, target detection can be achieved through a simple threshold segmentation. Experiments validate each component in our framework and show that our approach significantly and consistently outperforms all the state-of-the-art methods.

ACKNOWLEDGMENT

The authors would like to thank all the anonymous reviewers for their constructive comments on this letter.

REFERENCES

[1] X. Shao, H. Fan, G. Lu, and J. Xu, "An improved infrared dim and small target detection algorithm based on the contrast mechanism of human visual system," *Infr. Phys. Technol.*, vol. 55, no. 5, pp. 403–408, Sep. 2012.

[2] C. Q. Gao, D. Meng, Y. Yang, Y. Wang, X. Zhou, and A. G. Hauptmann, "Infrared patch-image model for small target detection in a single image," *IEEE Trans. Image Process.*, vol. 22, no. 12, pp. 4996–5009, Dec. 2013.

[3] I. S. Reed, R. M. Gagliardi, and L. B. Stotts, "Optical moving target detection with 3-D matched filtering," *IEEE Trans. Aerosp. Electron. Syst.*, vol. AES-24, no. 4, pp. 327–336, Jul. 1988.

[4] Y. Dai and Y. Wu, "Reweighted infrared patch-tensor model with both nonlocal and local priors for single-frame small target detection," *IEEE J. Sel. Topics Appl. Earth Observ. Remote Sens.*, vol. 10, no. 8, pp. 3752–3767, Aug. 2017.

[5] S. D. Deshpande, M. H. Er, R. Venkateswarlu, and P. Chan, "Max-mean and max-median filters for detection of small targets," *Proc. SPIE*, vol. 3809, pp. 74–83, Oct. 1999.

[6] J.-F. Rivest and R. Fortin, "Detection of dim targets in digital infrared imagery by morphological image processing," *Opt. Eng.*, vol. 35, no. 7, pp. 1886–1893, Jul. 1996.

[7] X. Bai and F. Zhou, "Analysis of new top-hat transformation and the application for infrared dim small target detection," *Pattern Recognit.*, vol. 43, no. 6, pp. 2145–2156, 2010.

[8] Y. He, M. Li, J. Zhang, and Q. An, "Small infrared target detection based on low-rank and sparse representation," *Infr. Phys. Technol.*, vol. 68, pp. 98–109, Jan. 2015.

[9] S. Kim, Y. Yang, J. Lee, and Y. Park, "Small target detection utilizing robust methods of the human visual system for IRST," *J. Infr., Millim., Terahertz Waves*, vol. 30, no. 9, pp. 994–1011, Sep. 2009.

[10] X. Wang, G. Lv, and L. Xu, "Infrared dim target detection based on visual attention," *Infr. Phys. Technol.*, vol. 55, no. 6, pp. 513–521, Nov. 2012.

[11] X. Dong, X. Huang, Y. Zheng, L. Shen, and S. Bai, "Infrared dim and small target detecting and tracking method inspired by human visual system," *Infr. Phys. Technol.*, vol. 62, pp. 100–109, Jan. 2014.

[12] J. Han, Y. Ma, J. Huang, X. Mei, and J. Ma, "An infrared small target detecting algorithm based on human visual system," *IEEE Geosci. Remote Sens. Lett.*, vol. 13, no. 3, pp. 452–456, Mar. 2016.

[13] H. Deng, X. Sun, M. Liu, C. Ye, and X. Zhou, "Small infrared target detection based on weighted local difference measure," *IEEE Trans. Geosci. Remote Sens.*, vol. 54, no. 7, pp. 4204–4214, Jul. 2016.

[14] C. L. P. Chen, H. Li, Y. Wei, T. Xia, and Y. Y. Tang, "A local contrast method for small infrared target detection," *IEEE Trans. Geosci. Remote Sens.*, vol. 52, no. 1, pp. 574–581, Jan. 2014.

[15] J. Han, Y. Ma, B. Zhou, F. Fan, K. Liang, and Y. Fang, "A robust infrared small target detection algorithm based on human visual system," *IEEE Geosci. Remote Sens. Lett.*, vol. 11, no. 12, pp. 2168–2172, Dec. 2014.

[16] Y. Wei, X. You, and H. Li, "Multiscale patch-based contrast measure for small infrared target detection," *Pattern Recognit.*, vol. 58, pp. 216–226, Oct. 2016.